Appendix:
Measuring the Slowly Evolving Trend in US Inflation with Professional Forecasts[†]

Gregor W. Smith
Department of Economics
94 University Avenue
Queen's University
Kingston, Ontario
CANADA K7L 3N6
email: smithgw@econ.queensu.ca

James M. Nason[‡]
Department of Economics
Campus Box 8110
NC State University
Raleigh, NC
U.S.A. 27695–8110
email: jmnason@ncsu.edu

April 26, 2020

[†]**This Appendix Is Not Intended for Publication.**

[‡]Acknowledgements: We thank the Social Sciences and Humanities Research Council of Canada, the Bank of Canada research fellowship programme, and the Jenkins Family Economics Fund of North Carolina State University for support of this research. The views expressed herein are not necessarily those of the Bank of Canada and are the authors' alone.

Appendix

The appendix has three sections. The first section constructs the rational expectations (RE) and sticky information (SI) state space models (SSMs) the paper estimates. The second section describes the data and Bayesian sequential Monte Carlo (SMC) methods used to estimate the SSMs. The SMC methods consist of a Metropolis-Hastings (MH) Markov chain Monte Carlo (MCMC) sampler wrapped around a Rao-Blackwellized auxillary particle filter (APF). Rao-Blackwellization addresses the nonlinearities in the SSMs. The nonlinearities are created by stochastic volatility (SV) in our version of the Stock and Watson (2007) unobserved components (UC) model of inflation. As mentioned in the paper, we call this UC model the BNSW model. Several additional estimation issues are discussed in the third section.

A.1 Summaries of the BNSW model and the RE- and SI-SSMs

We build and estimate RE- and SI-SSMs under different assumptions about inflation expectations. The RE-SSM sets the h-quarter ahead inflation prediction of the average member of the Survey of Professional Forecasters (SPF), $\pi_{t,h}^{SPF}$, to the h-quarter ahead RE forecast of inflation, $\mathbf{E}_t\pi_{t+h}$, plus classical measurement error, $\sigma_{\psi,h}\psi_{h,t}$, where $\psi_{h,t} \sim \mathcal{N}(0, 1)$ and $h = 1, \ldots, \mathcal{H}$. The SI-SSM equates $\pi_{t,h}^{SPF}$ to a h-quarter ahead SI inflation forecast, $F_t\pi_{t+h}$, and $\sigma_{\psi,h}\psi_{h,t}$.

The RE- and SI-SSMs engage our BNSW model to generate realized inflation, π_t. Our BNSW model is standard with one exception. The standard elements are (*i*) π_t equals trend inflation, τ_t, plus gap inflation, ϵ_t, (*ii*) the evolution of the former latent variable is a random walk in which the innovation, η_t, is hit by a lag of trend inflation SV, $\xi_{\eta,t-1}$, and (*iii*) this SV and the SV of gap inflation, $\xi_{\upsilon,t}$, are governed by geometric random walks (in $\ln\xi_{\eta,t}^2$ and $\ln\xi_{\upsilon,t}^2$). We depart from the standard specification by making ϵ_t a first-order autoregression, AR(1), that has its innovation υ_t interacting with $\xi_{\upsilon,t-1}$.

Trend inflation and $\xi_{\eta,t}$ are integrated out of the RE-SSM. The reason is $\pi_{t,h}^{SPF}$ and π_t share τ_t by combining $\pi_{t,h}^{SPF} = \mathbf{E}_t\pi_{t+h} + \sigma_{\psi,h}\psi_{h,t}$ with the BNSW model. Thus, making the dependent variables of the $h = 1$ to $\mathcal{H}$ observation equations, $\pi_{t,h}^{SPF} - \pi_t$, leaves ϵ_t and $\xi_{\upsilon,t}$ as the only states of the RE-SSM.

The SI-SSM is also restricted by the common inflation trend. Although the dependent variables are the same as in the RE case, the SI law of motion of inflation forecasts adds to each SI observation equation a lag of its dependent variable, $\pi_{t-1,h}^{SPF} - \pi_{t-1}$, as a predetermined regressor, the negative of the first difference of inflation, $-\Delta\pi_t = -\xi_{\eta,t-1}\eta_t - \epsilon_t + \epsilon_{t-1}$, and a lag of $\psi_{h,t}$ in addition to ϵ_t and $\psi_{h,t}$. Hence, ϵ_t, $\xi_{\upsilon,t}$, $\xi_{\eta,t}$, and $\psi_{h,t}$, $h = 1, \ldots, \mathcal{H}$, are states of the SI-SSM.

A.1.a Our BNSW Model

We reproduce our version of the BNSW model of inflation, π_t,

$$\pi_t = \tau_t + \epsilon_t, \tag{A.1.1}$$

$$\tau_t = \tau_{t-1} + \xi_{\eta,t-1}\eta_t, \qquad \eta_t \sim \mathcal{N}(0,1), \tag{A.1.2}$$

$$\epsilon_t = \rho\epsilon_{t-1} + \xi_{\upsilon,t-1}\upsilon_t, \qquad \upsilon_t \sim \mathcal{N}(0,1), \tag{A.1.3}$$

$$\ln \xi^2_{\eta,t} = \ln \xi^2_{\eta,t-1} + \sigma_\eta \phi_{\eta,t}, \qquad \phi_{\eta,t} \sim \mathcal{N}(0,1), \tag{A.1.4}$$

$$\ln \xi^2_{\upsilon,t} = \ln \xi^2_{\upsilon,t-1} + \sigma_\upsilon \phi_{\upsilon,t}, \qquad \phi_{\upsilon,t} \sim \mathcal{N}(0,1). \tag{A.1.5}$$

Equation (A.1.1) decomposes π_t into τ_t and ϵ_t. As mentioned previously, τ_t follows a random walk with SV, which is equation (A.1.2). Equation (A.1.3) is the AR(1) with SV that generates ϵ_t, where the AR1 parameter $\rho \in (-1, 1)$. The geometric random walks (A.1.4) and (A.1.5) produce the SVs. We assume the standard normal innovations η_t, υ_t, $\phi_{\eta,t}$, and $\phi_{\upsilon,t}$ form a vector of martingale difference sequences on the filtration $\mathcal{F}_{t-1}$ for $t = 0, 1, 2, \ldots, \infty$, given initial conditions τ_0, ϵ_0, $\xi_{\eta,0}$, and $\xi_{\upsilon,0}$.

A.1.b The RE-SSM

Our BNSW model predicts $\mathbf{E}_t\pi_{t+h} = \tau_t + \rho^h\epsilon_t$ and implies $\tau_t = \pi_t - \epsilon_t$, where it is implicit the states are conditional on date t information. Substitute for τ_t to find $\mathbf{E}_t\pi_{t+h} = \pi_t + (\rho^h - 1)\epsilon_t$. Since our RE assumption is $\pi^{SPF}_{t,h} = \mathbf{E}_t\pi_{t+h} + \sigma_{\psi,h}\psi_{h,t}$, for $h = 1, \ldots, \mathcal{H}$, the result is

$$\Pi^{SPF}_{t,h} \equiv \pi^{SPF}_{t,h} - \pi_t = \left(\rho^h - 1\right)\epsilon_t + \sigma_{\psi,h}\psi_{h,t}, \quad \psi_{h,t} \sim \mathcal{N}(0,1). \tag{A.1.6}$$

Equation (A.1.6) is the hth observation equation of the RE-SSM. The dependent variable $\Pi^{SPF}_{t,h}$ is the anticipated h-quarter ahead accumulation of inflation anticipated by the average member of the SPF.

We build the system of observation equations for the RE-SSM

$$\Pi^{SPF}_t \equiv \begin{bmatrix} \pi^{SPF}_{t,1} - \pi_t \\ \pi^{SPF}_{t,2} - \pi_t \\ \pi^{SPF}_{t,3} - \pi_t \end{bmatrix} = \boldsymbol{\mathcal{C}}_{RE}\, S_{RE,t} + \boldsymbol{\mathcal{D}}_{RE}\, \Psi_{RE,t}, \quad \Psi_{RE,t} \sim \mathcal{N}\left(\mathbf{0}_{3\times 1}, \mathbf{I}_3\right), \tag{A.1.7}$$

by stacking the observation equation (A.1.6) for $\mathcal{H} = 3$, where $\boldsymbol{\mathcal{C}}_{RE} = [\rho - 1 \;\; \rho^2 - 1 \;\; \rho^3 - 1]'$, $S_{RE,t} = \epsilon_t$, $\boldsymbol{\mathcal{D}}_{RE}$ has the diagonal $[\sigma_{\psi,1} \;\; \sigma_{\psi,2} \;\; \sigma_{\psi,3}]'$ and zeros elsewhere, and $\Psi_{RE,t} = [\psi_{1,t} \;\; \psi_{2,t} \;\; \psi_{3,t}]'$. The state equations for RE-SSM are the AR(1) of equation (A.1.3) and geometric random walk (A.1.5).

A.1.c THE SI-SSM

Sticky information places a wedge between $\pi_{t,h}^{SPF}$ and $\mathbf{E}_t\pi_{t+h}$ besides measurement error. The wedge is tied to the assumption the average member of the SPF does not completely update to $\mathbf{E}_t\pi_{t+h}$ date by date. The decision not to update inflation forecasts fully reflect costs faced by a SI forecaster. The costs are summarized by the probability λ the current SI inflation forecast, $F_t\pi_{t+h}$, is held at the SI inflation forecast of the previous period, $F_{t-1}\pi_{t+h}$, instead of updating as RE predicts. The SI inflation forecast is updated to $\mathbf{E}_t\pi_{t+h}$ at probability $1-\lambda$. Thus, the SI law of motion of inflation forecasts is

$$F_t\pi_{t+h} \;=\; \lambda F_{t-1}\pi_{t+h} \;+\; (1-\lambda)\mathbf{E}_t\pi_{t+h}, \tag{A.1.8}$$

where $1/(1-\lambda)$ is the frequency at which the SI forecaster updates $F_t\pi_{t+h}$ on average, given $\lambda \in (0,\, 1)$.

The observation equations of the SI-SPF SSM relies on $\mathbf{E}_t\pi_{t+h}$ computed by our BNSW model and its restriction on the first difference of π_t. We substitute for $\mathbf{E}_t\pi_{t+h}$ in the SI law of motion (A.1.8) to obtain $\left(1-\lambda\mathbf{L}\right)F_t\pi_{t+h} = (1-\lambda)\left[\tau_t \;+\; \rho^h\epsilon_t\right]$. Equation (A.1.1) of our BNSW model is used to replace τ_t in the previous expression giving us $\left(1-\lambda\mathbf{L}\right)F_t\pi_{t+h} = (1-\lambda)\left[\pi_t + \left(\rho^h-1\right)\epsilon_t\right]$. Next, move π_t and $\lambda F_{t-1}\pi_{t+h}$ to opposite sides of the equality to obtain $F_t\pi_{t+h} - \pi_t = \lambda\left(F_{t-1}\pi_{t+h} - \pi_t\right) + (1-\lambda)\left(\rho^h-1\right)\epsilon_t$. Finally, add and subtract π_{t-1} on the right side of the previous equation and recognize that $\Delta\pi_t = \xi_{\eta,t-1}\eta_t - (\epsilon_t - \epsilon_{t-1})$ using the BNSW model to produce the SI observation equation

$$\Pi_t^{SPF} \;=\; \lambda\Pi_{t-1}^{SPF} \;+\; \left[(1-\lambda)\rho^h - 1\right]\epsilon_t + \lambda\epsilon_{t-1} \;-\; \lambda\xi_{\eta,t-1}\eta_t \;+\; \sigma_{\psi,h}\psi_{h,t} \;-\; \lambda\sigma_{\psi,h}\psi_{h,t-1}. \tag{A.1.9}$$

Use $\pi_{t,h}^{SPF} = F_t\pi_{t+h} + \sigma_{\psi,h}\psi_{h,t}$ to eliminate $F_t\pi_{t+h}$ and $F_{t-1}\pi_{t+h}$ from the observation equation (A.1.9).

By piling up the SI observation equation (A.1.9) for $h = 1$, 2, and 3, we have the system of observation equations

$$\Pi_t^{SPF} \;=\; \boldsymbol{C}_{SI,t}\, S_{SI,t} \;-\; \lambda\,\xi_{\eta,t-1}\,\eta_t\,\mathbf{I}_3, \tag{A.1.10}$$

where $S_{SI,t} = \left[\epsilon_t \;\delta_{1,t} \;\delta_{2,t} \;\delta_{3,t} \;-\lambda\zeta_{1,t} \;-\lambda\zeta_{2,t} \;-\lambda\zeta_{3,t} \;\lambda\right]'$, $\delta_{t,h} = \epsilon_{t-1} + \zeta_{h,t} - \lambda\zeta_{h,t-1}$, $\zeta_{h,t} = \sigma_{\psi,h}\psi_{h,t}$,

$$\boldsymbol{C}_{SI,t} \;=\; \begin{bmatrix} (1-\lambda)\rho \;-1 & 1 & 0 & 0 & 0 & 0 & 0 & \Pi_{t-1,1}^{SPF} \\ (1-\lambda)\rho^2 - 1 & 0 & 1 & 0 & 0 & 0 & 0 & \Pi_{t-1,2}^{SPF} \\ (1-\lambda)\rho^3 - 1 & 0 & 0 & 1 & 0 & 0 & 0 & \Pi_{t-1,3}^{SPF} \end{bmatrix},$$

and $\Pi^{SPF}_{t-1,h} = \pi^{SPF}_{t-1,h} - \pi_{t-1}$. Creating $\delta_{h,t}$ and $\zeta_{h,t}$ and including these variables in the SI-state vector avoids having to estimate $\psi_{t,4}$ and its scale volatility, $\sigma_{\psi,4}$. However, this comes at the cost of losing the 4-quarter ahead average SPF inflation prediction in the observation equations of the RE- and SI-SSMs. The system of state equations of the SI-SSM is

$$S_{SI,t} \;=\; \boldsymbol{\mathcal{A}}_{SI}\, S_{SI,t-1} \;+\; \boldsymbol{\mathcal{B}}_{SI,t}\, \mathcal{E}_{SI,t}, \tag{A.1.11}$$

and the random walks of the SVs of trend and gap inflation, in $\ln \xi^2_{\eta,t}$ and $\ln \xi^2_{\upsilon,t}$, which are equations (A.1.4) and (A.1.5) of our BNSW model, where

$$\boldsymbol{\mathcal{A}}_{SI} \;=\; \left[\begin{array}{c:c:c:c} \rho & \mathbf{0}_{1\times 3} & \mathbf{0}_{1\times 3} & 0 \\ \hdashline \lambda \mathbf{1}_{3\times 1} & \mathbf{0}_{3\times 3} & \mathbf{I}_3 & 0 \\ \hdashline 0 & \mathbf{0}_{3\times 3} & \mathbf{0}_{3\times 3} & 0 \\ \hdashline 0 & \mathbf{0}_{1\times 3} & \mathbf{0}_{1\times 3} & 1 \end{array}\right], \qquad \boldsymbol{\mathcal{B}}_{SI,t} \;=\; \left[\begin{array}{c:c} \xi_{\upsilon,t-1} & \mathbf{0}_{1\times 3} \\ \hdashline \mathbf{0}_{3\times 1} & \mathbf{I}_3 \\ \hdashline \mathbf{0}_{3\times 1} & -\lambda \mathbf{I}_3 \\ \hdashline 0 & \mathbf{0}_{1\times 3} \end{array}\right],$$

$\mathcal{E}_{SI,t} = [\upsilon_t \;\; \zeta_{1,t} \;\; \zeta_{2,t} \;\; \zeta_{3,t}]'$, and the state system covariance matrix $\boldsymbol{\mathcal{B}}_{SI,t}\mathbf{E}_t\left\{\mathcal{E}_{SI,t}\mathcal{E}'_{SI,t}\right\}\boldsymbol{\mathcal{B}}'_{SI,t}$ is

$$\boldsymbol{\mathcal{Q}}_{SI,t} \;=\; \begin{bmatrix} \xi^2_{\upsilon,t-1} & 0 & 0 & 0 & 0 & 0 & 0 & 0 \\ 0 & \sigma^2_{\psi,1} & 0 & 0 & -\lambda\sigma^2_{\psi,1} & 0 & 0 & 0 \\ 0 & 0 & \sigma^2_{\psi,2} & 0 & 0 & -\lambda\sigma^2_{\psi,2} & 0 & 0 \\ 0 & 0 & 0 & \sigma^2_{\psi,3} & 0 & 0 & -\lambda\sigma^2_{\psi,3} & 0 \\ 0 & -\lambda\sigma^2_{\psi,1} & 0 & 0 & \lambda^2\sigma^2_{\psi,1} & 0 & 0 & 0 \\ 0 & 0 & -\lambda\sigma^2_{\psi,2} & 0 & 0 & \lambda^2\sigma^2_{\psi,2} & 0 & 0 \\ 0 & 0 & 0 & -\lambda\sigma^2_{\psi,3} & 0 & 0 & \lambda^2\sigma^2_{\psi,3} & 0 \\ 0 & 0 & 0 & 0 & 0 & 0 & 0 & 0 \end{bmatrix}. \tag{A.1.12}$$

Since the last element of $S_{SI,t}$ is the fixed SI parameter λ, the (7,7) element of $\boldsymbol{\Sigma}_{SI,t}$ is zero.

A.2. Estimating the RE- and SI-SSMs

This section describes the data and Bayesian SMC methods used to estimate the RE- and SI-SSMs. As in the paper, we refer to the RE- and SI-SSMs as $\mathcal{M}_{RE}$ and $\mathcal{M}_{SI}$. Estimation of $\mathcal{M}_{RE}$ and $\mathcal{M}_{SI}$ is performed on the software platform *Julia*, v1.1.0.

A.2.a The Data

The states and parameters of $\mathcal{M}_{RE}$ and $\mathcal{M}_{SI}$ are estimated on two samples. A sample consists of realized CPI or realized GNP/GDP deflator (PGNP/PGDP) inflation and associated average SPF inflation predictions. The CPI (PGNP/PGDP) sample is $1981Q4$–$2018Q4$ ($1969Q1$–$2018Q4$), $T = 149$ ($T = 200$). The RE- and SI-term structures of anticipated h-quarter accumulated SPF inflation predictions are limited to $h = 1, 2, 3$. The dependent variables Π_t^{SPF} cannot have $\pi_{t,4}^{SPF}$ because it requires $\pi_{t-1,4}^{SPF}$ as part of the predetermined variable in the SI observation equation (A.1.9). The SPF does not record 5-quarter ahead inflation predictions. Our measure of π_t is the fifth definition of realized CPI and PGNP/PGDP inflation in the `SPF forecast error statistics` spreadsheets compiled by the Real-Time Data Research Center of the Federal Reserve Bank of Philadelphia in the CPI-SPF data and PDNP/PDGP-SPF data. These webpages also have average CPI-SPF and PGNP/PGDP-SPF inflation predictions.

A.2.b Rao-Blackwellization of the RE- and SI-SSMs

Nonlinearities in $\mathcal{M}_{RE}$ and $\mathcal{M}_{SI}$ are created by the SVs of trend and gap inflation. Inflation gap SV creates a nonlinearity in the state equation (A.1.3) of $\mathcal{M}_{RE}$. However, this state equation yields conditionally linear and Gaussian estimates of $S_{RE,t+1}$ given knowledge of $\xi_{\upsilon,t}$. The same holds true for $S_{SI,t+1}$ in the state equation (A.1.11). Also, the SI observation equation (A.1.10) is linear and Gaussian, given $\xi_{\eta,t}$. The suggests breaking the state vectors of $\mathcal{M}_{RE}$ and $\mathcal{M}_{SI}$ into linear and nonlinear elements.

The process of creating a conditionally linear and Gaussian SSM out of a nonlinear SSM is referred to as Rao-Blackwellization (RB). Conditional on realizations of the SV(s), the RB step lets us apply the Kalman filter to integrate $S_{m,t}$ out of $\mathcal{M}_m$, $m = RE, SI$. Suppose $j = 1, \ldots, J$ draws or particles of $S_{m,t-1}^{(j)}$ are available. The RB step "mixes together" as many Kalman filters to compute the conditional distribution $S_{m,t|t} \sim \mathcal{N}\left(S_{m,t|t}^{(j)}, \mathbf{\Sigma}_{m,t|t}^{(j)}\right)$, where $\mathbf{\Sigma}_{m,t|t}^{(j)}$ is the mean square error (MSE) of $S_{m,t}^{(j)}$. This explains Chen and Liu (2000) calling a RB-particle filter that marginalizes $S_{m,t}$ a mixture Kalman filter; also see Creal (2012; section 2.5.7). Since the distribution of $S_{m,t}$ is computed analytically, the sampling error of the simulator is reduced; see Chen and Liu (2000), Creal (2012), and Särkkä (2013).

Only two steps have to be added to RB a bootstrap particle filter (BPF). First, given Π_t^{SPF}, Θ_{RE}, $\xi_{\upsilon,t-1}^{(j)}$, $S_{RE,t-1|t-1}^{(j)}$, and $\mathbf{\Sigma}_{RE,t-1|t-1}^{(j)}$, run the Kalman filter on $\mathcal{M}_{RE}$ to generate $S_{RE,t|t}^{(j)}$ and $\mathbf{\Sigma}_{RE,t|t}^{(j)}$ for each $j = 1, \ldots, \mathcal{J}$. In $\mathcal{M}_{RE}$, the RB-BPF updates the nonlinear state of gap inflation SV by treating the random walk law of motion (A.1.5) as a prior distribution from which to create $\left\{\xi_{\upsilon,t}^{(j)}\right\}_{j=1}^{\mathcal{J}}$ by simulation. In $\mathcal{M}_{SI}$, the prior at date $t-1$ depends on $\xi_{\eta,t-1}^{(j)}$, $\xi_{\upsilon,t-1}^{(j)}$, $S_{SI,t-1|t-1}^{(j)}$, and $\mathbf{\Sigma}_{SI,t-1|t-1}^{(j)}$. Updating of $S_{SI,t|t}^{(j)}$ and $\mathbf{\Sigma}_{SI,t|t}^{(j)}$ relies on the Kalman filter while simulating the random walk law of motion (A.1.4) yields $\left\{\xi_{\eta,t}^{(j)}\right\}_{j=1}^{\mathcal{J}}$.

The Kalman filter also yields an ensemble of log likelihoods, $\left\{\ell_{m,t}^{(j)}\right\}_{j=1}^{\mathcal{J}}$, that imply particle weights $\left\{\omega_{m,t}^{(j)}\right\}_{j=1}^{\mathcal{J}}$. These weights, which represent the contribution of a particle to the likelihood of $\mathcal{M}_m$ at date t, are $\omega_{m,t}^{(j)} = \exp\left\{\ell_{m,t}^{(j)}\right\} \Big/ \sum_{j=1}^{\mathcal{J}} \exp\left\{\ell_{m,t}^{(j)}\right\}$ for $j = 1, \ldots, \mathcal{J}$ and $m = RE, SI$. Next, resample $\left\{\omega_{m,t}^{(j)}\right\}_{j=1}^{\mathcal{J}}$ (with replacement) and record the indexes of the resampled weights to reorganize $\left\{S_{m,t|t}^{(j)}, \mathbf{\Sigma}_{m,t|t}^{(j)}, \xi_{\upsilon,t}^{(j)}\right\}_{j=1}^{\mathcal{J}}$. Thus, the BPF propagates without conditioning on information in Π_t^{SPF} to create ensembles of the date t linear and nonlinear states, $\left\{S_{m,t|t}^{(j)}, \mathbf{\Sigma}_{m,t|t}^{(j)}, \xi_{\upsilon,t}^{(j)}\right\}_{j=1}^{\mathcal{J}}$. Nonetheless, as the RB-BPF moves sequentially from date 1 to s, using the weights to resample reduces the chance of degeneracy in the particle stream $\left\{S_{m,t|t}^{(j)}, \mathbf{\Sigma}_{m,t|t}^{(j)}, \xi_{\upsilon,t}^{(j)}\right\}_{j=1}^{\mathcal{J}}$ for $s < t$, as $\mathcal{J} \longrightarrow \infty$.

A.2.c The RB-Auxiliary Particle Filter

Pitt and Shephard (1999, 2001) develop the APF to improve the efficiency of the simulator compared with the BPF; also see Creal (2012), and Särkkä (2013). The APF is an algorithm that first propagates and then resamples the states. The reason for reversing the order of these tasks compared with the BPF is to use information from the sample at date t to construct weights for resampling the date $t-1$ states. However, Johansen and Doucet (2008) and Creal (2012) discuss that the APF does not necessarily yield more efficient estimates of the states. Whether the APF yields more efficient estimates of the states depends on the distribution of the predictive likelihoods grounded in prior draws of the states having thinner tails compared with the distribution of the resampled predictive likelihoods.

Our RB-APF is a variation of algorithm 3 of Creal (2012, p. 267) and the procedures outlined in the appendix to Pitt, dos Santos Silva, Giordani, and Kohn (2012). The next algorithm implements our version of the RB-APF for $\mathcal{M}_{SI}$ conditional on Θ_{SI}.

1. Set $\varpi_{SI,0}^{(j)} = 1/\mathcal{J}$.

2. Draw $\mathcal{J}$ particles $\left\{S_{SI,0|0}^{(j)}, \mathbf{\Sigma}_{SI,0|0}^{(j)}, \xi_{\eta,0|0}^{(j)}, \xi_{\upsilon,0|0}^{(j)}\right\}_{j=1}^{\mathcal{J}}$ from the priors $S_{SI,0|0}^{(j)} \sim \mathcal{N}\left(S_{SI,0}, \mathbf{\Sigma}_{SI,0|0}\right)$,

$\boldsymbol{\Sigma}_{SI,0|0}^{(j)} = \boldsymbol{\Sigma}_{SI,0|0}$, $\ln\left[\xi_{\eta,0}^{(j)}\right]^2$, and $\ln\left[\xi_{\upsilon,0}^{(j)}\right]^2$, for $j = 1, \ldots, \mathcal{J}$.

3. At date $t = 1$ for $j = 1, 2, \ldots, \mathcal{J}$, run the Kalman filter prediction step on the conditionally linear and Gaussian system of observation and state equations (A.1.10) and (A.1.11) of $\mathcal{M}_{SI}$

$$\begin{aligned}
S_{SI,1|0}^{(j)} &= \boldsymbol{\mathcal{A}}_{SI}\, S_{SI,0|0}^{(j)}, \\
\boldsymbol{\Sigma}_{SI,1|0}^{(j)} &= \boldsymbol{\mathcal{A}}_{SI}\, \boldsymbol{\Sigma}_{SI,0|0}^{(j)} \boldsymbol{\mathcal{A}}_{SI}' + \boldsymbol{\mathcal{Q}}_{SI,0}^{(j)}, \\
\boldsymbol{\Omega}_{SI,1|0}^{(j)} &= \boldsymbol{C}_{SI,1}\, \boldsymbol{\Sigma}_{SI,1|0}^{(j)}\, \boldsymbol{C}_{SI,1}' + \boldsymbol{\mathcal{D}}_{SI,0}^{(j)} \boldsymbol{\mathcal{D}}_{SI,0}^{(j)\prime}, \\
\Pi_{SI,1}^{SPF\,(j)} &= \Pi_1^{SPF} - \boldsymbol{C}_{SI,1}\, S_{SI,1|0}^{(j)} \\
\ell_{SI,1}^{(j)} &= -\frac{1}{2}\left[\ln\left|\boldsymbol{\Omega}_{SI,1|0}^{(j)}\right| + \Pi_{SI,1}^{SPF\,(j)\prime}\, \mathrm{inv}\left(\boldsymbol{\Omega}_{SI,1|0}^{(j)}\right) \Pi_{SI,1}^{SPF\,(j)}\right],
\end{aligned}$$

where $\boldsymbol{\mathcal{Q}}_{SI,0}^{(j)}$ is defined by equation (A.1.12) and $\boldsymbol{\mathcal{D}}_{SI,0}^{(j)} = \lambda \xi_{\eta,0}^{(j)}$.

4. Reform the cloud of states into $\left\{\widetilde{S}_{SI,0|0}^{(j)}, \widetilde{\boldsymbol{\Sigma}}_{SI,0|0}^{(j)}, \widetilde{\xi}_{\eta,0}^{(j)}, \widetilde{\xi}_{\upsilon,0}^{(j)}\right\}_{j=1}^{\mathcal{J}}$ using indexes found by stratified resampling with replacement of the first stage particle weights $\varpi_{SI,0|1} = \dfrac{\omega_{SI,0|1}^{(j)}}{\sum_{j=1}^{\mathcal{J}} \omega_{SI,0|1}^{(j)}}$, where $\omega_{SI,0|1}^{(j)} = \dfrac{\varpi_{SI,0}^{(j)} \exp\left\{\ell_{SI,1}^{(j)}\right\}}{\sum_{j=1}^{\mathcal{J}} \varpi_{SI,0}^{(j)}}$; see Hol, Schön, and Gustafsson (2006) and Li, Bolic, and Djuric (2015).

5. Draw from $\left\{\widetilde{S}_{SI,0|0}^{(j)}, \widetilde{\boldsymbol{\Sigma}}_{SI,0|0}^{(j)}, \widetilde{\xi}_{\eta,0}^{(j)}, \widetilde{\xi}_{\upsilon,0}^{(j)}\right\}_{j=1}^{\mathcal{J}}$ to run the entire Kalman filter algorithm

$$\begin{aligned}
S_{SI,1|0}^{(j)} &= \boldsymbol{\mathcal{A}}_{SI}\, \widetilde{S}_{SI,0|0}^{(j)}, \\
\boldsymbol{\Sigma}_{SI,1|0}^{(j)} &= \boldsymbol{\mathcal{A}}_{SI}\, \widetilde{\boldsymbol{\Sigma}}_{SI,0|0}^{(j)} \boldsymbol{\mathcal{A}}_{SI}' + \widetilde{\boldsymbol{\mathcal{Q}}}_{SI,0}^{(j)}, \\
\boldsymbol{\Omega}_{SI,1|0}^{(j)} &= \boldsymbol{C}_{SI,1}\, \boldsymbol{\Sigma}_{SI,1|0}^{(j)}\, \boldsymbol{C}_{SI,1}' + \widetilde{\boldsymbol{\mathcal{D}}}_{SI,0}^{(j)} \widetilde{\boldsymbol{\mathcal{D}}}_{SI,0}^{(j)\prime}, \\
\Pi_{SI,1}^{SPF\,(j)} &= \Pi_1^{SPF} - \boldsymbol{C}_{SI,1}\, S_{SI,1|0}^{(j)} \\
\ell_{SI,1}^{(j)} &= -\frac{1}{2}\left[\ln\left|\boldsymbol{\Omega}_{SI,1|0}^{(j)}\right| + \Pi_{SI,1}^{SPF\,(j)\prime}\, \mathrm{inv}\left(\boldsymbol{\Omega}_{SI,1|0}^{(j)}\right) \Pi_{SI,1}^{SPF\,(j)}\right], \\
\boldsymbol{\mathcal{K}}_{SI,1}^{(j)} &= \boldsymbol{\mathcal{A}}_{SI}\, \boldsymbol{\Sigma}_{SI,1|0}^{(j)}\, \boldsymbol{C}_{SI,1}'\, \mathrm{inv}\left(\boldsymbol{\Omega}_{SI,1|0}^{(j)}\right), \\
S_{SI,1|1}^{(j)} &= S_{1|0}^{(j)} + \boldsymbol{\mathcal{K}}_{SI,1}^{(j)}\, \widetilde{\Pi}_{SI,1}^{SPF}, \\
\boldsymbol{\Sigma}_{SI,1|1}^{(j)} &= \boldsymbol{\Sigma}_{SI,1|0}^{(j)} - \boldsymbol{\Sigma}_{SI,1|0}^{(j)}\, \boldsymbol{C}_{SI,1}'\, \mathrm{inv}\left(\boldsymbol{\Omega}_{SI,1|0}^{(j)}\right) \boldsymbol{C}_{SI,1}\, \boldsymbol{\Sigma}_{SI,1|0}^{(j)}.
\end{aligned}$$

6. Compute second stage weights, $\varpi_{SI,1}^{(j)} = \dfrac{\omega_{SI,1}^{(j)}}{\sum_{j=1}^{\mathcal{J}} \omega_{SI,1}^{(j)}}$, for $j = 1, \ldots, \mathcal{J}$, where $\omega_{SI,1}^{(j)} = \exp\left\{ \ell_{SI,1}^{(j)} - \widetilde{\ell}_{SI,1}^{(j)} \right\}$ and resampling of the first stage predictive log likelihoods, $\left\{ \widetilde{\ell}_{SI,1}^{(j)} \right\}_{j=1}^{\mathcal{J}}$, is done the same way as for the states in step 4.

7. Generate $\mathcal{J}$ realizations of the trend and inflation gap SVs, $\ln\left[\xi_{\eta,1}^{(j)}\right]^2$ and $\ln\left[\xi_{\upsilon,1}^{(j)}\right]^2$, using the independent random walks (A.1.4) and (A.1.5) conditional on $\left\{\ln\left[\widetilde{\xi}_{\eta,0}^{(j)}\right]^2, \ln\left[\widetilde{\xi}_{\upsilon,0}^{(j)}\right]^2\right\}_{j=1}^{\mathcal{J}}$, and $\mathcal{J}$ draws from two independent standard normal distributions.

8. Pass $\left\{ S_{SI,1|1}^{(j)}, \boldsymbol{\Sigma}_{SI,1|1}^{(j)}, \widetilde{\xi}_{\eta,1}^{(j)}, \widetilde{\xi}_{\upsilon,1}^{(j)} \right\}_{j=1}^{\mathcal{J}}$ to repeat the algorithm for steps 2 to 7 at $t = 2, 3, \ldots, T$,

   (a) Use the observation and state equations (A.1.10) and (A.1.11) of $\mathcal{M}_{SI}$ to operate the Kalman filter prediction step

$$
\begin{aligned}
S_{SI,t|t-1}^{(j)} &= \boldsymbol{\mathcal{A}}_{SI}\, S_{SI,t-1|t-1}^{(j)}, \\
\boldsymbol{\Sigma}_{SI,t|t-1}^{(j)} &= \boldsymbol{\mathcal{A}}_{SI}\, \boldsymbol{\Sigma}_{SI,t-1|t-1}^{(j)} \boldsymbol{\mathcal{A}}_{SI}' + \boldsymbol{\mathcal{Q}}_{SI,t-1}^{(j)}, \\
\boldsymbol{\Omega}_{SI,t|t-1}^{(j)} &= \boldsymbol{C}_{SI,t}\, \boldsymbol{\Sigma}_{SI,t|t-1}^{(j)} \boldsymbol{C}_{SI,t}' + \boldsymbol{\mathcal{D}}_{SI,t-1}^{(j)} \boldsymbol{\mathcal{D}}_{SI,t-1}^{(j)\prime}, \\
\Pi_{SI,t}^{SPF\,(j)} &= \Pi_{t-1}^{SPF} - \boldsymbol{C}_{SI,t}\, S_{SI,t|t-1}^{(j)}, \\
\ell_{SI,t}^{(j)} &= -\frac{1}{2}\left[\ln\left|\boldsymbol{\Omega}_{SI,t|t-1}^{(j)}\right| + \Pi_{SI,t}^{SPF\,(j)\prime}\, \mathrm{inv}\left(\boldsymbol{\Omega}_{SI,t|t-1}^{(j)}\right) \Pi_{SI,t}^{SPF\,(j)} \right].
\end{aligned}
$$

   where $\boldsymbol{\mathcal{Q}}_{SI,t-1}^{(j)}$ is defined by equation (A.1.12) and $\boldsymbol{\mathcal{D}}_{SI,t-1}^{(j)} = \lambda \xi_{\eta,t-1}^{(j)}$.

   (b) Resample (with replacement) the states using the ensemble of first stage weights $\left\{ \varpi_{t-1|t}^{(j)} \right\}_{j=1}^{\mathcal{J}}$ to produce $\left\{ \widetilde{S}_{SI,t|t}^{(j)}, \widetilde{\boldsymbol{\Sigma}}_{SI,t|t}^{(j)}, \widetilde{\xi}_{\eta,t}^{(j)}, \widetilde{\xi}_{\upsilon,t}^{(j)} \right\}_{j=1}^{\mathcal{J}}$, where $\varpi_{t-1|t}^{(j)} = \dfrac{\omega_{SI,t-1|t}^{(j)}}{\sum_{j=1}^{\mathcal{J}} \omega_{SI,t-1|t}^{(j)}}$ and $\omega_{SI,t-1|t}^{(j)} = \dfrac{\varpi_{SI,t-1}^{(j)}}{\sum_{j=1}^{\mathcal{J}} \varpi_{SI,t-1}^{(j)}} \exp\left\{ \ell_{SI,t}^{(j)} \right\}$.

(c) Employ the resampled states in the Kalman filter filter operations

$$
\begin{aligned}
S_{SI,t|t-1}^{(j)} &= \mathcal{A}_{SI}\, \widetilde{S}_{SI,t-1|t-1}^{(j)}, \\
\boldsymbol{\Sigma}_{SI,t|t-1}^{(j)} &= \mathcal{A}_{SI}\, \widetilde{\boldsymbol{\Sigma}}_{SI,t-1|t-1}^{(j)} \mathcal{A}_{SI}' + \widetilde{\mathcal{Q}}_{t-1}^{(j)}, \\
\boldsymbol{\Omega}_{SI,t|t-1}^{(j)} &= \boldsymbol{C}_{SI,t}\, \boldsymbol{\Sigma}_{SI,t|t-1}^{(j)} \boldsymbol{C}_{SI,t}' + \widetilde{\mathcal{D}}_{SI,t-1}^{(j)} \widetilde{\mathcal{D}}_{SI,t-1}^{(j)\prime}, \\
\Pi_{SI,t}^{SPF\,(j)} &= \Pi_t^{SPF} - \boldsymbol{C}_{SI,t}\, S_{SI,t|t-1}^{(j)}, \\
\ell_{SI,t}^{(j)} &= -\frac{1}{2}\left[\ln\left| \boldsymbol{\Omega}_{SI,t|t-1}^{(j)} \right| + \Pi_t^{SPF\,(j)\prime}\, \mathrm{inv}\left(\boldsymbol{\Omega}_{SI,t|t-1}^{(j)} \right) \Pi_t^{SPF\,(j)} \right], \\
\boldsymbol{\mathcal{K}}_{SI,t}^{(j)} &= \mathcal{A}_{SI}\, \boldsymbol{\Sigma}_{SI,t|t-1}^{(j)} \boldsymbol{C}_{SI,t}'\, \mathrm{inv}\left(\boldsymbol{\Omega}_{SI,t|t-1}^{(j)} \right), \\
S_{SI,t|t}^{(j)} &= S_{SI,t|t-1}^{(j)} + \boldsymbol{\mathcal{K}}_{SI,t}^{(j)} \widetilde{\Pi}_{SI,t}^{(j)}, \\
\boldsymbol{\Sigma}_{SI,t|t}^{(j)} &= \boldsymbol{\Sigma}_{SI,t|t-1}^{(j)} - \boldsymbol{\Sigma}_{SI,t|t-1}^{(j)} \boldsymbol{C}_{SI,t}'\, \mathrm{inv}\left(\boldsymbol{\Omega}_{SI,t|t-1}^{(j)} \right) \boldsymbol{C}_{SI,t}\, \boldsymbol{\Sigma}_{SI,t|t-1}^{(j)},
\end{aligned}
$$

(d) For $j = 1, \ldots, \mathcal{J}$, use $\omega_{SI,t}^{(j)} = \exp\left\{ \ell_{SI,t}^{(j)} - \widetilde{\ell}_{SI,t}^{(j)} \right\}$ to form the second stage weights, $\varpi_{SI,t}^{(j)} = \omega_{SI,t}^{(j)} \big/ \sum_{j=1}^{\mathcal{J}} \omega_{SI,t}^{(j)}$.

(e) Employ the independent random walks (A.1.4) and (A.1.5) to draw $\mathcal{J}$ particles of the nonlinear states $\xi_{\eta,t}^{(j)}$ and $\xi_{\upsilon,t}^{(j)}$, given the resampled particles $\left\{ \widetilde{\xi}_{\eta,t-1}^{(j)}, \widetilde{\xi}_{\upsilon,t-1}^{(j)} \right\}_{j=1}^{\mathcal{J}}$, and two new independent samples of $\mathcal{J}$ standard normal random numbers.

9. The filtered distribution of $\xi_{k,t}$ conditional on $\left\{ \widetilde{\xi}_{k,t-1}^{(j)} \right\}_{j=1}^{\mathcal{J}}$, $\Pi_{1:t}^{SPF}$, $\mathcal{M}_{SI}$ and Θ_{SI},

$$
\mathcal{P}\left(\xi_{k,t} \,\middle|\, \widetilde{\xi}_{k,t-1},\, \Pi_{1:t}^{SPF},\, \mathcal{M}_{SI};\, \Theta_{SI} \right),
$$

is approximated by the discrete distribution of particles $\left\{ \xi_{k,t}^{(j)} \right\}_{j=1}^{\mathcal{J}}$ using the *pdf* of $\left\{ \omega_{SI,t-1|t}^{(j)} \right\}_{j=1}^{\mathcal{J}}$ for $k = \eta, \upsilon$. The associated filtered distribution of $S_{SI,t}$ is approximated by a mixture of normal distributions $\mathcal{N}\left(S_{SI,t|t}^{(j)}, \boldsymbol{\Sigma}_{SI,t|t}^{(j)} \right)$ with the same *pdf*. Thus, the filtered means of $S_{SI,t|t}$, $\boldsymbol{\Sigma}_{SI,t|t}$, $\xi_{\eta,t}$ and $\xi_{\upsilon,t}$ are calculated as $S_{SI,t|t} = \sum_{j=1}^{\mathcal{J}} \varpi_{SI,t}^{(j)} S_{SI,t|t}^{(j)}$, $\boldsymbol{\Sigma}_{SI,t|t} = \sum_{j=1}^{\mathcal{J}} \varpi_{SI,t}^{(j)} \boldsymbol{\Sigma}_{SI,t|t}^{(j)}$, $\xi_{\eta,t} = \sum_{j=1}^{\mathcal{J}} \varpi_{SI,t}^{(j)} \xi_{\eta,t}^{(j)}$, and $\xi_{\upsilon,t} = \sum_{j=1}^{\mathcal{J}} \varpi_{SI,t}^{(j)} \xi_{\upsilon,t}^{(j)}$.

10. The likelihood of $\mathcal{M}_m$ is estimated at date t using

$$\mathcal{P}\left(\Pi_t^{SPF} \middle| \Pi_{1:t-1}^{SPF};\ \mathcal{M}_m,\ \Theta_m\right) = \left(\frac{1}{\mathcal{J}}\sum_{j=1}^{\mathcal{J}} \omega_{m,t}^{(j)}\right) \sum_{j=1}^{\mathcal{J}} \omega_{m,t-1|t}^{(j)}, \tag{A.2.1}$$

for $m = RE, SI$, which replicates equation (17) of Pitt, et al (2012).

A.2.d A Random Walk PMH-MCMC

Our SMC simulator relies on unbiased estimates of the likelihood of a SSM to construct posterior distributions of its parameters. Andrieu, Doucet, and Holenstein (2010) show the posterior distributions produced by a MH-MCMC are unaffected by the estimation error that results from computing a likelihood, $\mathfrak{L}\left(\Pi_{1:T}^{SPF} \middle| \Theta_m,\ \mathcal{M}_m\right) = \exp\left\{\sum_{t=1}^{T} \ln \mathcal{P}\left(\Pi_t^{SPF} \middle| \Pi_{1:t-1}^{SPF};\ \mathcal{M}_m,\ \Theta_m\right)\right\}$, using equation (A.2.1), as long as it is unbiased. Conditions for a particle filter to produce unbiased estimates of the likelihood are discussed by Andrieu, Doucet, and Holenstein (2010). They call the combination of a MH-MCMC and a particle filer a particle (P)MH-MCMC algorithm.

These results motivate us to create a PMH-MCMC by wrapping a random walk MH-MCMC simulator around our Rao-Blackwellized-APF. We implement a PMH-MCMC algorithm to generate posterior distributions of $S_{m,t}$, $\mathbf{\Sigma}_{m,t}$, $\xi_{\eta,t}$, $\xi_{\upsilon,t}$, and Θ_m for $m = RE, SI$ following the advice of Pitt, dos Santos Silva, Giordani, and Kohn (2012), Doucet, Pitt, Deligiannidis, and Kohn (2015), and Martino, Elvira, and Camps-Valls (2018).

A problem is PMH-MCMC samplers can be computationally complex and costly. Pitt, dos Santos Silva, Giordani, and Kohn (2012) propose a solution. The solution calculates the optimal trade-off between the computational costs of increasing the number particles, $\mathcal{J}$, against the benefit of a higher acceptance rate in the PMH-MCMC. The stopping rule for determining the optimal $\mathcal{J}$ relies on the variance in the error of the log likelihood of a SSM. The practical issue is that Pitt dos Santos Silva, Giordani, and Kohn ground their analysis in the assumption the proposal of the MH-MCMC is ideal. Since access to an ideal proposal is rare, Doucet, Pitt, Deligiannidis, and Kohn (2015) suggest a reasonable value of $\mathcal{J}$ is one that produces an error variance of the log likelihood equal to 1.2^2.

We follow their advice and a procedure outlined by Pitt, dos Santos Silva, Giordani, and Kohn (2012) to calibrate $\mathcal{J}$. First, we run the PMH-MCMC on $\mathcal{M}_{RE}$ and $\mathcal{M}_{SI}$ with a large $\mathcal{J}$ and a small number of steps to obtain an estimates close to the posterior means of Θ_{RE} and Θ_{SI}. Next, $\mathcal{M}_{RE}$ and $\mathcal{M}_{SI}$ are

simulated on a grid of particles that ranges from only a few, say, 26, to several hundred conditional on the posterior mean, $\overline{\Theta}_m$. At each point on the grid, compute the simulated log likelihood of $\mathcal{M}_m$. Choose $\mathcal{J}$ to set the standard deviation of the error of the log likelihood to be about 1.2.

The PMH-MCMC algorithm consists of the following steps.

1. Draw the initial parameter estimates, $\widehat{\Theta}_{m,0}$, to generate $\widehat{\mathcal{L}}\left(\Pi_{1:T}^{SPF} \middle| \widehat{\Theta}_{m,0}, \mathcal{M}_m\right)$ using the RB-APF algorithm and likelihood (A.2.1) for $m = RE, SI$.

2. Create the proposed update of $\widehat{\Theta}_{m,0}$, $\Theta_{m,1}$, using the multivariate MH random walk law of motion,

$$\Theta_{m,1} = \widehat{\Theta}_{m,0} + \Gamma_{\Theta,m,0}^{1/2} \vartheta_{m,1},$$

where $\Gamma_{\Theta_m,0}^{1/2}$ is the Cholesky decomposition of an initial draw of the covariance matrix of Θ_m, $\Gamma_{\Theta_m,0}$ $\sim \left(2.4 \Big/ \sqrt{d_m}\right)^2 \mathcal{IW}\left(100.0, 0.01\mathbf{I}_{d_m}\right)$, $\vartheta_{m,1} \sim \mathcal{N}\left(0_{d_m \times 1}, \mathbf{I}_{d_m}\right)$, and $d_m = \dim\left(\Theta_m\right)$.

3. Calculate the MH criterion $\alpha_1 = \min\left\{\dfrac{\widehat{\mathcal{L}}\left(\Pi_{1:T}^{SPF} \middle| \Theta_{m,1}, \mathcal{M}_m\right) q\left(\Theta_{m,0}, \Theta_{m,1}\right) \mathcal{P}\left(\Theta_{m,1}\right)}{\widehat{\mathcal{L}}\left(\Pi_{1:T}^{SPF} \middle| \widehat{\Theta}_{m,0}, \mathcal{M}_m\right) q\left(\Theta_{m,1}, \Theta_{m,0}\right) \mathcal{P}\left(\widehat{\Theta}_{m,0}\right)}, 1\right\}$, where running the RB-APF produces $\widehat{\mathcal{L}}\left(\Pi_{1:T}^{SPF} \middle| \Theta_{m,1}, \mathcal{M}_m\right)$, $q(\cdot, \cdot)$ is the kernel of the proposal distribution, and $\mathcal{P}\left(\Theta_{m,1}\right)$ and $\mathcal{P}\left(\widehat{\Theta}_{m,0}\right)$ are priors located at $\Theta_{m,1}$ and $\widehat{\Theta}_{m,1}$, respectively.

4. Draw a uniform random variable $\nu_1 \sim \mathcal{U}(0, 1)$. If $\nu_1 \leq \alpha_1$, set $\widehat{\Theta}_{m,1} = \Theta_{m,1}$ and the counter π to one. Otherwise, $\widehat{\Theta}_{m,1} = \widehat{\Theta}_{m,0}$ and $\pi = 0$.

5. For $i = 2, 3, \ldots, \mathcal{K}$, repeat steps 2, 3, and 4 using the MH random walk law of motion

$$\Theta_{m,k} = \widehat{\Theta}_{m,k-1} + \Gamma_{\Theta,m,k-1}^{1/2} \vartheta_{m,k}, \quad \vartheta_{m,k} \sim \mathcal{N}\left(0_{d_m \times 1}, \mathbf{I}_{d_m}\right),$$

to test $\alpha_i = \min\left\{\dfrac{\widehat{\mathcal{L}}\left(\Pi_{1:T}^{SPF} \middle| \Theta_{m,k}, \mathcal{M}_m\right) q\left(\Theta_{m,k-1}, \Theta_{m,k}\right) \mathcal{P}\left(\Theta_{m,k}\right)}{\widehat{\mathcal{L}}\left(\Pi_{1:T}^{SPF} \middle| \widehat{\Theta}_{m,k-1}, \mathcal{M}_m\right) q\left(\Theta_{m,k}, \Theta_{m,k-1}\right) \mathcal{P}\left(\widehat{\Theta}_{m,k-1}\right)}, 1\right\}$ against a uniform random variable $\nu_i \sim \mathcal{U}\left(0, 1\right)$. If $\nu_i \leq \alpha_i$, we have $\widehat{\Theta}_{m,k} = \Theta_{m,k}$. Otherwise, $\widehat{\Theta}_{m,k} = \widehat{\Theta}_{m,k-1}$. The latter decision holds the counter at π while the former outcome updates π to $\pi + 1$.

Part of the output of the PMH-MCMC is $\left\{\widehat{\Theta}_{m,k}, \widehat{\mathcal{L}}\left(\Pi_{1:T}^{SPF} \middle| \widehat{\Theta}_{m,k}, \mathcal{M}_m\right)\right\}_{k=1}^{\mathcal{K}}$. These parameter draws and likelihoods characterize the posterior distribution of $\mathcal{M}_m$, given the prior $\mathcal{P}\left(\Theta_m\right)$.

The kernel of the proposal distribution, $q(\cdot, \cdot)$, appears in the MH ratio in steps 3 and 5. The reason is the support of the targets and proposals of Θ_m differ. The latter have support on the (whole) real line because $\vartheta_m \sim \mathcal{N}(0_{d_m \times 1}, \mathbf{I}_{d_m})$. The targets of $\rho \in (-1, 1)$, σ_υ, $\sigma_{\psi,h} \in (0, \infty)$, and $\lambda \in (0, 1)$ have bounded support. Lindström (2017) shows $q(\cdot, \cdot)$ is the gradient of the target restricted by its support, where the proposal is a function of the target using the natural logarithm.

A.3 Additional Computing Issues

The PMH-MCMC inserts a simulator, the RB-APF, into another simulator, a MCMC sampler. This leaves us with choices to make for the number of steps in the MCMC sampler, $\mathcal{K}$, and for every step k the number of particles, $\mathcal{J}$, to implement the RB-APF. Our choice of $\mathcal{K}$ is driven by the oft cited goal of producing posterior distributions of Θ_{RE} and Θ_{SI} that are approximately serially uncorrelated.

We set $\mathcal{J}$ guided by theory developed and methods proposed by Pitt, et al (2012) and Doucet, Pitt, Deligiannidis, and Kohn (2015). As previously mentioned, Pitt et al provide theory to choose the optimal number of particles by setting the error variance of the estimated log likelihood to the theoretical optimum. However, the theory is grounded on the assumption that the proposal of the PMH-MCMC is an exact match for the target (*i.e.*, the posterior) distribution. By relaxing this requirement, Doucet et al are able to construct a theoretical upper bound on computing time that trades it for the error variance of the estimated log likelihood of a particle filter to set $\mathcal{J} = \mathcal{J}^\star$. The upper bound gives a stopping rule that ties $\mathcal{J}^\star$ to the error variance of the estimated log likelihood, $\hat{\sigma}^2_{\mathcal{L},m}$, that approximates 1.2^2.

1. Following the advice of Doucet et al, we implement the stopping rule in two steps.

   (a) Pitt et al suggest the $\overline{\Theta}_m$ needed to calculate $\mathcal{J}^\star$ can be obtained by using a large number of particles and a small number of MCMC steps. We follow this advice by inputting 100,000 particles for the RB-APF at each of the 30,000 steps on which the PMH-MCMC is run. A third of the MCMC steps are discarded as a burn-in sample to produce an estimate of the posterior mean, $\overline{\Theta}_m$ for $\mathcal{M}_m$, $m = RE, SI$, on the SPF-CPI and SPF-PGNP/PGDP inflation samples.

   (b) When $\mathcal{J} = 100{,}000$, the PMH-MCMC is run in parallel. In this case, we engage the distributed parallel PMH-MCMC algorithm of Martino, Elvira, and Camps-Valls (2018) to estimate $\overline{\Theta}_m$. This task is given to a workstation running Ubuntu 18.04.2 that has an Intel® Xeon® W–2155 CPU with 10 cores and 20 threads. The PMH-MCMC is run by splitting the $\mathcal{J}$ particles evenly

across the 20 threads using the Julia (v1.1.0) command `pmap`. Martino, et al discuss the way in which the 20 unbiased likelihood estimates can be combined to provide the needed input to calculate the MH criterion for updating the posterior of $\mathcal{M}_m$.

(c) Given an estimate of $\overline{\Theta}_m$, we run the RB-APF to estimate $\hat{\mathfrak{L}}\left(\Pi_{1:T}^{SPF} \middle| \overline{\Theta}_m, \mathcal{M}_m\right)$ on a sequence of particles starting at $\mathcal{J} = 26$, adding a particle at a time, and stopping when $\hat{\sigma}^2_{\hat{\mathfrak{L}},m}$ is less than or equal to 1.2. This number of particles is labeled $\mathcal{J}^\star$.

(d) On the CPI-SPF sample, $\mathcal{J}_m^\star$ equals 50 and 112 for $m = RE$ and SI. These rise to $\mathcal{J}_{RE}^\star = 63$ and $\mathcal{J}_{SI}^\star = 171$ on the PGNP/PGDP-SPF sample. The PMH-MCMC is run on a single thread for $\mathcal{M}_{RE}$ and $\mathcal{M}_{SI}$ on the two samples across the calibrated values of $\mathcal{J}_m^\star$.

2. The prior of $\ln \xi_{\upsilon,0}^2$ affects initial conditions of the linear states, $S_{m,0|0}$, and MSE, $\mathbf{\Sigma}_{m,0}$, where $m = RE, SI$. We draw $S_{RE,0|0}^{(j)} \sim \mathcal{N}\left(S_{RE,0}, \mathbf{\Sigma}_{RE,0}\right)$, where $S_{RE,0} = 0$ because the unconditional mean of gap inflation is zero and $j = 1, \ldots, \mathcal{J}$. Its MSE is $\mathbf{\Sigma}_{RE,0} = \mathbf{E}\left\{\left[\xi_{\upsilon,0|0}^{(j)}\right]^2\right\} \Big/ \left(1 - \rho_0^2\right)$, where $\mathbf{E}\left\{\left[\xi_{\upsilon,0|0}^{(j)}\right]^2\right\}$ is the mean of $\mathcal{J}$ draws from the prior of $\ln \xi_{\upsilon,0}^2$ and ρ_0 is the initial proposal for the AR1 parameter of gap inflation. Similarly, the unconditional means of the measurement errors, $\psi_{h,t}$, are zero leading to $S_{SI,0} = \mathbf{0}_{2\mathcal{H}+1,1}$. Solving $\text{var}(\mathbf{\Sigma}_{SI,0}) = \mathcal{A}_{SI}\,\text{var}(\mathbf{\Sigma}_{SI,0})\mathcal{A}_{SI}' + \mathcal{B}_{SI,0}\,\text{var}(\mathcal{E}_{SI,0})\mathcal{B}_{SI,0}'$ yields $\mathbf{\Sigma}_{SI,0}$ in which the (1,1) element of $\mathcal{B}_{SI,0}$ is $\sqrt{\mathbf{E}\left\{\left[\xi_{\upsilon,0|0}^{(j)}\right]^2\right\}}$. Otherwise, $\mathcal{B}_{SI,0}$ matches $\mathcal{B}_{SI,t}$ in equation (A.1.12) element by element. These results make it possible to draw $S_{SI,0|0}^{(j)} \sim \mathcal{N}\left(S_{SI,0}, \mathbf{\Sigma}_{SI,0}\right)$.

3. The PGNP/PGDP-SPF inflation sample is missing several observations for $h = 4$. Since $\pi_{t-1,3}^{SPF}$ is part of a dependent variable in the system of observation equations (A.1.10) of $\mathcal{M}_{SI}$, the Kalman filter is employed to forecast these missing observations. We adopt a forecasting procedure discussed in Durbin and Koopman (2012). Within the RB-APF, the Kalman filter updating equations are used to produce a forecast of $\Pi_{t,3}^{SPF}$. Carrying this forecast over to date $t+1$ fills in the missing observation when needed.

4. We adopt robust adaptive Metropolis (RAM) algorithm of Vihola (2012) to estimate the covariance matrix of the target distribution, $\Theta_{m,k}$, $m = RE, SI$ and $k = 1, \ldots, \mathcal{K}$.

(a) The RAM algorithm does not produce an empirical covariance matrix of the target. Instead, it aims to achieve the desired acceptance rate of the proposal, $\alpha^\star$, in a random walk MCMC by

adding a matrix with positive diagonal elements to the Cholesky decomposition of a previous estimate of the covariance matrix. The result is an estimate of the covariance matrix that is guaranteed to be positive definite and unique; see Särkkä (2013). Vihola (2012) also argues the RAM algorithm is robust to thick tailed targets.

(b) The inputs into the RAM algorithm are innovations of the proposed updates, ϑ_k, at step k, $\alpha^\star$, and the Cholesky decomposition of the covariance matrix of $\Theta_{m,k}$ computed in the previous step, $\Gamma^{1/2}_{\Theta,m,k-1}$. The RAM estimate of the covariance matrix is

$$\Gamma_{\Theta,m,k} = \Gamma^{1/2}_{\Theta,m,k-1}\Gamma^{1/2\prime}_{\Theta,m,k-1} + \Gamma^{1/2}_{\Theta,m,k-1}\left(\min\left(1, d_m k^{\iota}\right) \times (\alpha_k - \alpha^\star)\frac{\vartheta_k \vartheta_k'}{||\vartheta_k||^2}\right)\Gamma^{1/2\prime}_{\Theta,m,k-1},$$

where ι is the step size to adapt new proposals. Vihola suggests $\iota \approx -0.65$. We set $\alpha^\star$ to the optimal acceptance rate (0.234) of a MH-MCMC with a multivariate target.

(c) We compute $\Gamma_{\Theta,m,k}$ at every step of the burn-in. When making draws from the posterior, if $\alpha_k < 0.23$ or $\alpha_k > 0.238$ at $k = 1, \ldots, \mathcal{K}$, $\Gamma_{\Theta,m,k}$ is updated.

5. The PMH-MCMC is operated for a burn-in phase of $\mathcal{K}_{BRN} = 750{,}000$ steps, where $\hat{\Theta}_{m,0} = \overline{\Theta}_m$. Subsequently, we let the PMH-MCMC sampler run for $\mathcal{K} = 1{,}500{,}000$ steps to construct posterior estimates of $\mathcal{M}_{RE}$ and $\mathcal{M}_{SI}$ on the the SPF-CPI inflation and SPF-PGDP/GNP inflation samples.

6. The posterior draws are highly correlated. We thin the posterior distributions using the statistically efficient algorithm of Owen (2017). The algorithm selects an efficient thinning factor by trading the costs of updating the MCMC sampler and computing the likelihood of $\mathcal{M}_m$ for less serial correlation in the posterior distribution of Θ_m.

   (a) The statistically efficient thinning factor is 12, given a maximal first-order auto-correlation coefficient of 0.963 across the posteriors of $\hat{\Theta}_{RE}$ and $\hat{\Theta}_{SI}$ on the two samples and a cost of computing the likelihood that is a third of the cost of updating the PMH-MCMC sampler.

   (b) This yields 125,000 posterior draws. The thinned posterior distributions of $\hat{\Theta}_{RE}$ and $\hat{\Theta}_{SI}$ have first-order auto-correlation coefficients less than 0.640.

7. We evaluate the SI hypothesis by comparing marginal data densities (MDD) of $\mathcal{M}_{RE}$ and $\mathcal{M}_{SI}$ on the CPI-SPF and PGNP/PGDP-SPF samples.

(a) The posterior densities of $\hat{\Theta}_{RE}$ or $\hat{\Theta}_{SI}$, which are conditional on the data and our priors, are building blocks for the MDDs. The PMH-MCMC is the tool used to construct posterior distributions of $\mathcal{M}_{RE}$ and $\mathcal{M}_{SI}$. Using Bayes rule, model priors, $\mathcal{P}\left(\Theta_m\right)$, and likelihoods are linked to the posterior of $\hat{\Theta}_m$ according to

$$\mathcal{P}\left(S_t,\ \Theta_m \left| \Pi_{1:T}^{SPF},\ \mathcal{M}_m\right.\right) \ \propto\ \mathcal{L}\left(\Pi_{1:T}^{SPF} \left| \Theta_m,\ \mathcal{M}_m\right.\right) \mathcal{P}\left(\Theta_m\right),$$

where $m = RE, SI$. Integrating Θ_m out of the likelihood

$$\mathcal{L}\left(\Pi_{1:T}^{SPF} \left| \mathcal{M}_m\right.\right) \ =\ \int \mathcal{L}\left(\Pi_{1:T}^{SPF} \left| \Theta_m,\ \mathcal{M}_m\right.\right) \mathcal{P}\left(\Theta_m\right) d\Theta_m,$$

produces the MDD, which is conditional on $\mathcal{M}_m$, m = RE, SI. We calculate log MDDs with the harmonic mean method, which is discussed in Geweke (2005, pp. 248–261); also see Gelfand and Dey (1994), Geweke (1998), and Fernández-Villaverde and Rubio-Ramírez (2004). Geweke (2005) summarizes results in Gelfand and Dey (1994) that include

$$\frac{1}{\mathcal{L}\left(\Pi_{1:T}^{SPF} \left| \mathcal{M}_m\right.\right)} \ =\ \frac{1}{\mathcal{K}} \sum_{i=1}^{\mathcal{K}} \frac{\mathcal{G}\left(\Theta_{m,i}\right)}{\mathcal{L}\left(\Pi_{1:T}^{SPF} \left| \mathcal{M}_m\right.\right) \mathcal{P}\left(\Theta_{m,i}\right)}, \tag{A.2.2}$$

as $\mathcal{K} \longrightarrow \infty$, where $\mathcal{G}\left(\Theta_{m,i}\right)$ is a probability density evaluated at $\Theta_{m,i}$.

(b) A useful approach to computing the probability density $\mathcal{G}\left(\cdot\right)$ is proposed by Geweke (1998). His approach instructs us to compute

$$\mathcal{G}\left(\Theta_{m,i}\right) \ =\ \frac{(2\pi)^{-0.5d}}{\varrho} \left|\boldsymbol{\Omega}_{\Theta_m}\right|^{0.5} \exp\left\{-0.5\left(\Theta_{m,i} - \hat{\Theta}_m\right) \boldsymbol{\Omega}_{\Theta_m}^{-1} \left(\Theta_{m,i} - \hat{\Theta}_m\right)'\right\} \mathtt{I}_{\Theta_m^{\dagger} \cap \Theta_{m,i}}\left(\Theta_{m,i}\right),$$

using the output of the PMH-PMCMC, where $\Omega_{\Theta_m} \ =\ \frac{1}{\mathcal{K}} \sum_{i=1}^{\mathcal{K}} \left(\Theta_{m,i} - \hat{\Theta}_m\right) \left(\Theta_{m,i} - \hat{\Theta}_m\right)'$, ϱ is the significance level chosen to restrict the compact set

$$\Theta_m^{\dagger} \ =\ \left\{\Theta_{m,i} : \left(\Theta_{m,i} - \hat{\Theta}_m\right) \boldsymbol{\Omega}_{\Theta_m}^{-1} \left(\Theta_{m,i} - \hat{\Theta}_m\right)' \leq \chi^2_{1-\varrho}(d)\right\},$$

and $\mathtt{I}_{\Theta_m^{\dagger} \cap \Theta_{m,i}}\left(\Theta_{m,i}\right)$ is an indicator function that equals one when $\Theta_m^{\dagger} \bigcap \Theta_{m,i}$ is true. Thus, $\mathcal{G}\left(\Theta_{m,i}\right)$ is well described by a truncated multivariate normal distribution with mean $\hat{\Theta}_{m,i}$ and covariance matrix $\boldsymbol{\Omega}_{\Theta_m}$ because of the restrictions created by $\mathtt{I}_{\Theta_m^{\dagger} \cap \Theta_{m,i}}\left(\Theta_{m,i}\right)$ and $\Theta_{m,j}^{\dagger}$.

Moreover, the compact set $\Theta_m^\dagger$ bounds $\mathcal{P}\left(S_t,\ \Theta_m \middle| \Pi_{1:T}^{SPF},\ \mathcal{M}_m\right)$ from above. When the posterior is also bounded away from zero on $\Theta_m^\dagger$, the reciprocal of the arithmetic mean of $\exp\left\{\mathcal{L}\left(\Pi_{1:T}^{SPF} \middle| \mathcal{M}_m\right)\right\}$ is efficiently approximated by employing $\mathcal{G}\left(\Theta_{m,i}\right)$ to normalize the appropriate posterior at each of the $i = 1, 2, \ldots, \mathcal{K}$ steps and average the result.

(c) The PMH-MCMC produces the output necessary to conduct model evaluation using the posterior odds ratio. We compute $\left\{\mathcal{G}\left(\Theta_{m,i}\right)\right\}_{i=1}^{\mathcal{K}}$, grab the associated $\left\{\mathcal{L}\left(\Pi_{1:T}^{SPF} \middle| \mathcal{M}_m\right)\right\}_{i=1}^{\mathcal{K}}$ and $\left\{\mathcal{P}\left(\Theta_{m,i}\right)\right\}_{i=1}^{\mathcal{K}}$, and use (A.2.2) to compute the harmonic mean of $\mathcal{L}\left(\Pi_{1:T}^{SPF} \middle| \mathcal{M}_m\right)$ for $m = RE$, SI. The posterior odds ratio, which produces evidence about the views the data have about $\mathcal{M}_{RE}$ and $\mathcal{M}_{SI}$, is calculated using $\mathcal{L}\left(\Pi_{1:T}^{SPF} \middle| \mathcal{M}_{RE}\right)$, $\mathcal{P}\left(\Theta_{RE,i}\right)$, $\mathcal{L}\left(\Pi_{1:T}^{SPF} \middle| \mathcal{M}_{SI}\right)$, and $\mathcal{P}\left(\Theta_{SI,i}\right)$ on each of the two samples.

8. We report filtered estimates of trend inflation, $\tau_{i,t|t} = \pi_t - \epsilon_{i,t|t}$ for $i = 1, \ldots, \mathcal{K}$. These estimates are constructed conditional on the posterior draws from $\widehat{\Theta}_{RE}$ or $\widehat{\Theta}_{SI}$ across the CPI-SPF and GNP/GDP-SPF samples. Using RB-APF estimates of gap inflation does not alter these estimates.

9. Along with this trend-gap inflation decomposition, our BNSW model (A.1.1)–(A.1.5) assumes the innovations to trend and gap inflation, η_t and υ_t, are uncorrelated at all leads and lags. This lets us construct a posterior distribution for trend inflation SV, $\xi_{\eta,t}$, in $\mathcal{M}_{RE}$ using $\left\{\{\tau_{i,t|t}\}_{i=1}^{\mathcal{K}}\right\}_{t=1}^{T}$, the prior of $\ln \xi_{\eta,0}^2$, and a prior on τ_0.

(a) Treat $\left\{\{\tau_{i,t|t}\}_{i=1}^{\mathcal{K}}\right\}_{t=1}^{T}$ as known. This creates a SSM consisting of the observation equation $\ln(\tau_t - \tau_{t-1})^2 = \ln \xi_{\eta,t-1}^2 + \ln \eta_t^2$ and the random walk (A.1.4) is the state equation. This SSM is linear and non-Gaussian. Harvey, Ruiz, and Shephard (1994) point out that, although $\ln \eta_t^2$ is non-Gaussian, its first and second moments are $\mathbf{E} \ln \eta_t^2 = -1.27$ and $\mathbf{E}\left\{\ln \eta_t^2\right\}^2 = 0.5 \times \pi^2$.

(b) We use these facts and that the Kalman gain of $\ln\left[\xi_{\eta,t}\right]^2$ is fixed at $\gamma_\pi = 2.0/(2.0 + \pi^2)$ to write its Kalman filter updating equation as

$$\ln \xi_{\eta,i,t}^2 \ = \ 1.27 \ + \ (1.0 - \gamma_\pi) \ln \xi_{\eta,i,t-1}^2 \ + \ \gamma_\pi \ln\left[(\tau_{i,t} - \tau_{i,t-1})(\tau_{i,t} - \tau_{i,t-1})\right],$$

for $i = 1, \ldots, \mathcal{K}$, where $\ln \xi_{\eta,0}^2$ is drawn from its prior described in table 2, we choose the prior $\tau_0 \sim \mathcal{N}\left(\mu_\pi, 30.0^2\right)$, and μ_π is the average inflation rate on the ten years before the start of the CPI-SPF or the PGNP/PGDP-SPF sample. The posterior distribution of $\left\{\xi_{\eta,i,t}\right\}_{i=1}^{\mathcal{K}}$

is created for $t = 1, \ldots, T$ by making $\mathcal{K}$ draws from these initial conditions and the posterior distribution of τ_t.

10. The posterior distribution of σ_η is built in a similar fashion for $\mathcal{M}_{RE}$. Since the random walk (A.1.4) can be written as $\sigma_\eta \phi_{\eta,t} = \left(\ln \xi^2_{\eta,t} - \ln \xi^2_{\eta,t-1}\right)$, $\widehat{\sigma}_{\eta,i} = \sqrt{T^{-1} \sum_{t=1}^{T} \left(\ln \xi^2_{\eta,i,t} - \ln \xi^2_{\eta,i,t-1}\right)^2}$ for $i = 1, \ldots, \mathcal{K}$, where $\ln \xi^2_{\eta,i,0}$ is drawn from its prior.

11. Quantiles and uncertainty bands of the fixed model parameters, trend inflation, gap inflation, the SVs, and measurement errors are grounded in the posterior distribution of $\mathcal{M}_{RE}$ and $\mathcal{M}_{SI}$ on the CPI-SPF and PGNP/PGDP-SPF samples.

    (a) The figures in the paper and appendix are created in *Julia* v1.1.0 using its *PyPlot* and *PyCall* packages along with *Python* v3.6 and *Matplotlib* v3.1.1.

    (b) Medians of the posterior distributions and uncertainty bands are reported in figures 2 and 4 of the paper and figures A.1 and A.2 shown at the end of this appendix. Uncertainty bands are computed using the plug-in sup-t statistic developed by Olea and Plagborg-Møller (2018).

    (c) We add a $T \times T$ matrix with means of the relevant MSEs down the diagonal and zeros elsewhere to the empirical covariance matrix (*i.e.*, outer product) of the posterior distributions of trend and gap inflation for $\mathcal{M}_{RE}$ and $\mathcal{M}_{SI}$ and $\psi_{h,t}$ in $\mathcal{M}_{SI}$.

    (d) The MSEs of trend inflation is obtained by running the Kalman filter on $\mathcal{M}_{RE}$ and $\mathcal{M}_{SI}$ altered for this purpose conditional on the posterior distributions of $\widehat{\Theta}_{RE}$ or $\widehat{\Theta}_{SI}$. The PMH-MCMC The MSEs are computed using the Kalman filter as described in section A.2.d.

    (e) For the SVs in both SSMs and the measurements errors of $\mathcal{M}_{RE}$, the uncertainty bands depend on a $T \times T$ empirical covariance matrix of the relevant posterior distribution.

12. Posterior moments of the measurement errors are reported in tables A.1, A.2, and A.3 and figures A.1 and A.2 of this appendix.

    (a) We back out posterior distributions of the measurement errors of $\mathcal{M}_{RE}$ using its observation equation (A.1.6), $\psi_{i,t,h} = \sigma^{-1}_{i,\psi,h} \left[\pi^{SPF}_{t,h} - \pi_t - \left(\rho^h_i - 1\right) \epsilon_{i,t}\right]$, for $h = 1, 2, 3$ and $i = 1, \ldots, \mathcal{K}$.

(b) Measurement errors are implicit state variables in $\mathcal{M}_{SI}$. For this reason, $\psi_{i,t,h}$ is found by adjusting posterior distributions of the state variable $-\lambda_i \zeta_{i,t,h}$ in $\mathcal{M}_{SI}$ using its posterior distributions of λ_i and $\sigma_{i,\psi,h}$.

(c) We examine the time series behavior of the posterior distributions of $\psi_{h,t}$, $h = 1, 2, 3$, across $\mathcal{M}_{RE}$ and $\mathcal{M}_{SI}$ on the CPI-SPF and PGNP/PGDP-SPF samples in tables A.1 to A.3 and figures A.1 and A.2 that appear at the end of this appendix.

(d) Tables A.1, A.2, and A.3 contain posterior moments of $\psi_{1,t}$, $\psi_{2,t}$, and $\psi_{3,t}$, respectively. The moments are the median standard deviation, $s(\psi_{h,t})$, median autocorrelations, ACF(ℓ), at lags $\ell = 1, 2, 3, 4$, and 8, mean Ljung-Box statistics with four and eight lags, and the associated Bayesian (*i.e.*, mean) p-values; see Gelman (2005). The ACFs are calculated in *Julia* (v1.1.0) using *PyCall* to call the *Python* (v3.6) module *StatsModels* v0.10.2 and its toolkit *stattools.tsa*. This toolkit has the function `acf` that computes ACFs using a fast Fourier transform. The tables also present five and 95 percent quantiles of $s(\psi_{h,t})$ and ACF(ℓ) in brackets.

(e) The median $s(\psi_{h,t})$s are not near one as shown in tables A.1, A.2, and A.3. The 90 percent Bayesian credible intervals of $s(\psi_{h,t})$ never contain one for $h = 1, 2, 3$. Just below these statistics in the tables are the median ACF(ℓ)s, which are often far from zero. Only 20 percent of the 90 percent Bayesian credible intervals include zero. Thus, it is not a surprise that in only two of 24 cases, do the mean Ljung-Box statistics have Bayesian p-values greater than 0.05. The two exceptions occur for $\psi_{2,t}$ in $\mathcal{M}_{SI}$ on the PGNP/PGDP-SPF sample at four and eight lags.

(f) Plots of the medians and 68 percent uncertainty bands of the posterior distributions of $\psi_{1,t}$, $\psi_{2,t}$, and $\psi_{3,t}$ appear in figures A.1 and A.2. The former figure contains median measurement errors and uncertainty bands produced by estimating $\mathcal{M}_{RE}$ on the CPI-SPF sample. The PGNP/PGDP-SPF sample and $\mathcal{M}_{SI}$ are responsible for the median estimates and uncertainty bands appearing in figure A.2. The figures consist of three panels that run from $h = 1$ at the top, $h = 2$ in the middle, and $h = 3$ at the bottom.

(g) Figure A.1 is consistent with the story told by tables A.1, A.2, and A.3. The probability is strong there is serial correlation present in the posterior distributions $\psi_{1,t}$, $\psi_{2,t}$, and $\psi_{3,t}$ associated with $\mathcal{M}_{RE}$ and the CPI-SPF sample.

(h) This is not the case for figure A.2. Its 68 percent uncertainty bands are wide for the $\psi_{1,t}$, $\psi_{2,t}$, and $\psi_{3,t}$ quarter by quarter from $1969Q1$ to $2018Q4$ in the PGNP/PGDP-SPF sample as produced by $\mathcal{M}_{SI}$. The uncertainty bands are broad enough to cover zero at every quarter. Hence, the plots in figure A.2 provide evidence of substantial uncertainty in the posterior estimates of these measurement errors. Remember the MSEs of these (implicit) state variables are used to construct the uncertainty bands. Hence, the MSEs capture substantial uncertainty in the posterior distribution of these measurement errors.

References

Andrieu, A., Doucet, A., & Holenstein, R. 2010. Particle Markov chain Monte Carlo methods. *Journal of the Royal Statistical Society, Series B* 72(3), 269–342.

Chen, R., & Liu, J.S. 2000. Mixture Kalman filters. *Journal of the Royal Statistical Society, Series B* 62(3), 493–508.

Coibion, O., & Gorodnichenko, Y. 2015. Information rigidity and the expectations formation process: A simple framework and new facts. *American Economic Review* 105(8), 2644–2678.

Creal D. 2012. A survey of sequential Monte Carlo methods for economics and finance. *Econometric Reviews* 31(3) 245–296.

Doucet, A., Pitt, M., Deligiannidis, G., & Kohn, R. 2015. Efficient implementation of Markov chain Monte Carlo when using an unbiased likelihood estimator. *Biometrika* 102(2), 295–313.

Durbin, J., & Koopman, S.J. 2012. Time Series Analysis by State Space Methods, Second Edition, Oxford, UK: Oxford University Press.

Fernández-Villaverde, J., & Rubio-Ramírez, J.F. 2004. Comparing dynamic equilibrium models to data: a Bayesian approach. *Journal of Econometrics* 123(1), 153–187.

Gelfand, A.E., & Dey, D.K. 1994. Bayesian model choice: Asymptotics and exact calculations. *Journal of the Royal Statistical Society B* 56(3) 501–514.

Gelman, A. 2005. Comment: Fuzzy and Bayesian $p-$values and $u-$values. *Statistical Science*, 20(4) 380–381.

Gelman, A., Carlin, J.B., Stern, H.S., & Rubin, DB. 2004. Bayesian Data Analysis, Second Edition, New York, NY: Chapman and Hall, CRC Press.

Geweke, J. 1998. Using simulation methods for Bayesian econometric models: inference, development, and communication. Staff Report 249, Federal Reserve Bank of Minneapolis.

Geweke, J. 2005. Contemporary Bayesian Econometrics and Statistics, Hoboken, NJ: J. Wiley and Sons, Inc.

Harvey, A., Ruiz, E., & Shephard, N. 1994. Multivariate stochastic variance models. *The Review of Economic Studies* 61(2), 247–264.

Hol, J.D., Schön, T.B., & Gustafsson, F. (2006). On resampling algorithms for particle filters. In IEEE NONLINEAR STATISTICAL SIGNAL PROCESSING WORKSHOP, Ng, W. (ed.), 79–82. Red Hook, NY: Curran Associates, Inc.

Johansen, A.M., & Doucet, A. 2008. A note on auxiliary particle filters. *Statistics and Probability Letters* 78(12), 1498–1504.

Lindström, J. 2017. Transformed proposal distributions. Manuscript, Centre for Mathematical Sciences, Lund University (available at `https://umbertopicchini.files.wordpress.com/2017/12/transformed-proposals2.pdf`).

Li, T., Bolic, M., & Djuric, P. 2015. Resampling methods for particle filtering: Classification, implementation, and strategies. *IEEE Signal Processing Magazine* 32(3), 70–86.

Martino, L., Elvira, V., & Camps-Valls, G. 2018. Group importance sampling for particle filtering and MCMC. *Digital Signal Processing* 82(1), 133–151.

Olea, J.L.M., & Plagborg-Møller, M. 2018. Simultaneous confidence bands: Theory, implementation, and an application to SVARs. *Journal of Applied Econometrics* 34(1), 1–17.

Owen, A.B. 2017. Statistically efficient thinning of a Markov chain sampler. *Journal of Computational and Graphical Statistics* 26(3), 738–744.

Pitt, M.K., dos Santos Silva, R., Giordani, P., & Kohn, R. 2012. On some properties of Markov chain Monte Carlo simulation methods based on the particle filter. *Journal of Econometrics* 171(2) 134–151.

Pitt, M.K., & Shephard, N. 2001. Auxiliary Variable Based Particle Filters. In Doucet, A., de Freitas, N., Gordon, N. (eds.) SEQUENTIAL MONTE CARLO METHODS IN PRACTICE, New York, NY: Springer-Verlag.

Pitt, M.K., & Shephard, N. 1999. Filtering via Simulation: Auxiliary Particle Filters. *Journal of the American Statistical Association* 94(446), 590–599.

Särkkä, S. 2013. BAYESIAN FILTERING AND SMOOTHING, Cambridge, UK: Cambridge University Press.

Stock J.H., & Watson, M.W. 2007. Why has US inflation become harder to forecast? *Journal of Money, Credit and Banking* 39(S1), 3–33.

Vihola, M. 2012. Robust adaptive Metropolis algorithm with coerced acceptance rate. *Statistics and Computing* 22(5), 997–1008.

Table A.1 Posterior Moments of Measurement Error at $h = 1$

	CPI Inflation Sample: $1981Q4$–$2018Q4$		GNP/GDP Deflator Inflation Sample: $1969Q1$–$2018Q4$	
	$\mathcal{M}_{RE}$	$\mathcal{M}_{SI}$	$\mathcal{M}_{RE}$	$\mathcal{M}_{SI}$
$s(\psi_{1,t})$	0.790 [0.727, 0.854]	0.652 [0.595, 0.706]	0.890 [0.829, 0.951]	0.629 [0.585, 0.676]
ACF(1)	−0.051 [−0.097, −0.002]	0.225 [0.165, 0.281]	0.071 [0.025, 0.123]	0.389 [0.328, 0.444]
ACF(2)	−0.021 [−0.054, 0.011]	−0.128 [−0.045, −0.074]	−0.057 [−0.069, −0.035]	0.132 [0.092, 0.176]
ACF(3)	−0.164 [−0.202, −0.119]	−0.145 [−0.180, −0.099]	−0.024 [−0.045, 0.013]	0.132 [0.093, 0.169]
ACF(4)	0.251 [0.225, 0.269]	0.115 [0.092, 0.142]	0.233 [0.230, 0.237]	0.241 [0.200, 0.263]
ACF(8)	0.187 [0.161, 0.209]	0.156 [0.056, 0.132]	0.035 [0.022, 0.048]	0.026 [0.001, 0.054]
$Q(4)$	14.453 (0.008)	15.859 (0.004)	13.162 (0.011)	50.116 (0.000)
$Q(8)$	20.502 (0.013)	18.482 (0.019)	15.752 (0.049)	55.553 (0.000)

The table presents posterior moments of the measurement error at $h = 1$. Since measurement error is a part of the state vector of the SI model, $\mathcal{M}_{SI}$, under this column the moments are created from the posterior of filtered measurement error, $\psi_{t|t,1}$. For the RE model, $\mathcal{M}_{SI}$, estimates of $\psi_{1,t}$ are backed out from the actual data, filtered gap inflation, and the posterior of the model parameters. The first row is the median of the posterior of the standard deviation of $\psi_{1,t}$, $s(\psi_{1,t})$. The median autocorrelation function at lag j is denoted ACF(j). Five and 95 percent quantiles appear in brackets. The mean posterior Ljung-Box statistic with q lags is in the row denoted $Q(q)$. The rows below $Q(4)$ and $Q(8)$ display Bayesian $p-$values in parentheses.

Table A.2 Posterior Moments of Measurement Error at $h = 2$

	CPI Inflation Sample: $1981Q4$–$2018Q4$		GNP/GDP Deflator Inflation Sample: $1969Q1$–$2018Q4$	
	$\mathcal{M}_{RE}$	$\mathcal{M}_{SI}$	$\mathcal{M}_{RE}$	$\mathcal{M}_{SI}$
$s(\psi_{2,t})$	0.464 [0.420, 0.511]	0.342 [0.311, 0.378]	0.599 [0.545, 0.656]	0.390 [0.361, 0.419]
ACF(1)	−0.586 [−0.616, −0.516]	0.058 [−0.148, 0.264]	−0.237 [−0.288, −0.176]	0.106 [−0.013, 0.221]
ACF(2)	0.487 [0.460, 0.503]	0.322 [0.286, 0.349]	−0.079 [−0.097, −0.066]	0.077 [0.046, 0.103]
ACF(3)	−0.456 [−0.498, −0.389]	−0.138 [−0.258, 0.001]	−0.129 [−0.137, −0.119]	−0.026 [−0.076, 0.027]
ACF(4)	0.482 [0.471, 0.490]	0.350 [0.295, 0.401]	0.206 [0.200, 0.211]	0.087 [0.051, 0.133]
ACF(8)	0.350 [0.312, 0.377]	0.248 [0.175, 0.321]	0.096 [0.080, 0.108]	0.090 [0.049, 0.137]
$Q(4)$	154.740 (0.000)	41.378 (0.000)	24.959 (0.000)	6.622 (0.219)
$Q(8)$	216.355 (0.000)	61.693 (0.000)	28.583 (0.001)	12.372 (0.170)

The table presents posterior moments of the measurement error at $h = 2$. See the notes to table A.1.

Table A.3 Posterior Moments of Measurement Error at $h = 3$

	CPI Inflation Sample: $1981Q4$–$2018Q4$		GNP/GDP Deflator Inflation Sample: $1969Q1$–$2018Q4$	
	$\mathcal{M}_{RE}$	$\mathcal{M}_{SI}$	$\mathcal{M}_{RE}$	$\mathcal{M}_{SI}$
$s(\psi_{3,t})$	0.664 [0.615, 0.717]	0.560 [0.509, 0.603]	0.785 [0.729, 0.841]	0.534 [0.494, 0.566]
ACF(1)	0.051 [−0.002, 0.107]	0.233 [0.173, 0.298]	0.257 [0.198, 0.318]	0.426 [0.365, 0.478]
ACF(2)	0.099 [0.044, 0.147]	−0.031 [−0.079, 0.016]	0.018 [−0.050, 0.085]	0.165 [0.108, 0.218]
ACF(3)	0.025 [−0.011, 0.062]	−0.060 [−0.086, −0.017]	0.013 [−0.038, 0.068]	0.164 [0.124, 0.201]
ACF(4)	0.315 [0.294, 0.333]	0.169 [0.140, 0.206]	0.230 [0.209, 0.253]	0.144 [0.116, 0.173]
ACF(8)	0.109 [0.093, 0.124]	−0.040 [−0.066, 0.007]	0.015 [−0.004, 0.034]	−0.050 [−0.083, −0.014]
$Q(4)$	17.585 (0.002)	13.980 (0.010)	25.373 (0.000)	52.661 (0.000)
$Q(8)$	24.303 (0.003)	16.669 (0.040)	30.511 (0.001)	54.239 (0.000)

The table presents posterior moments of the measurement error at $h = 3$. See the notes to table A.1.

Figure A.1: $\mathcal{M}_{RE}$ Estimates of Measurement Errors, $\psi_{h,t}$, for $h = 1$, 2, and 3, on the CPI-SPF Sample, 1981$Q4$ to 2018$Q4$

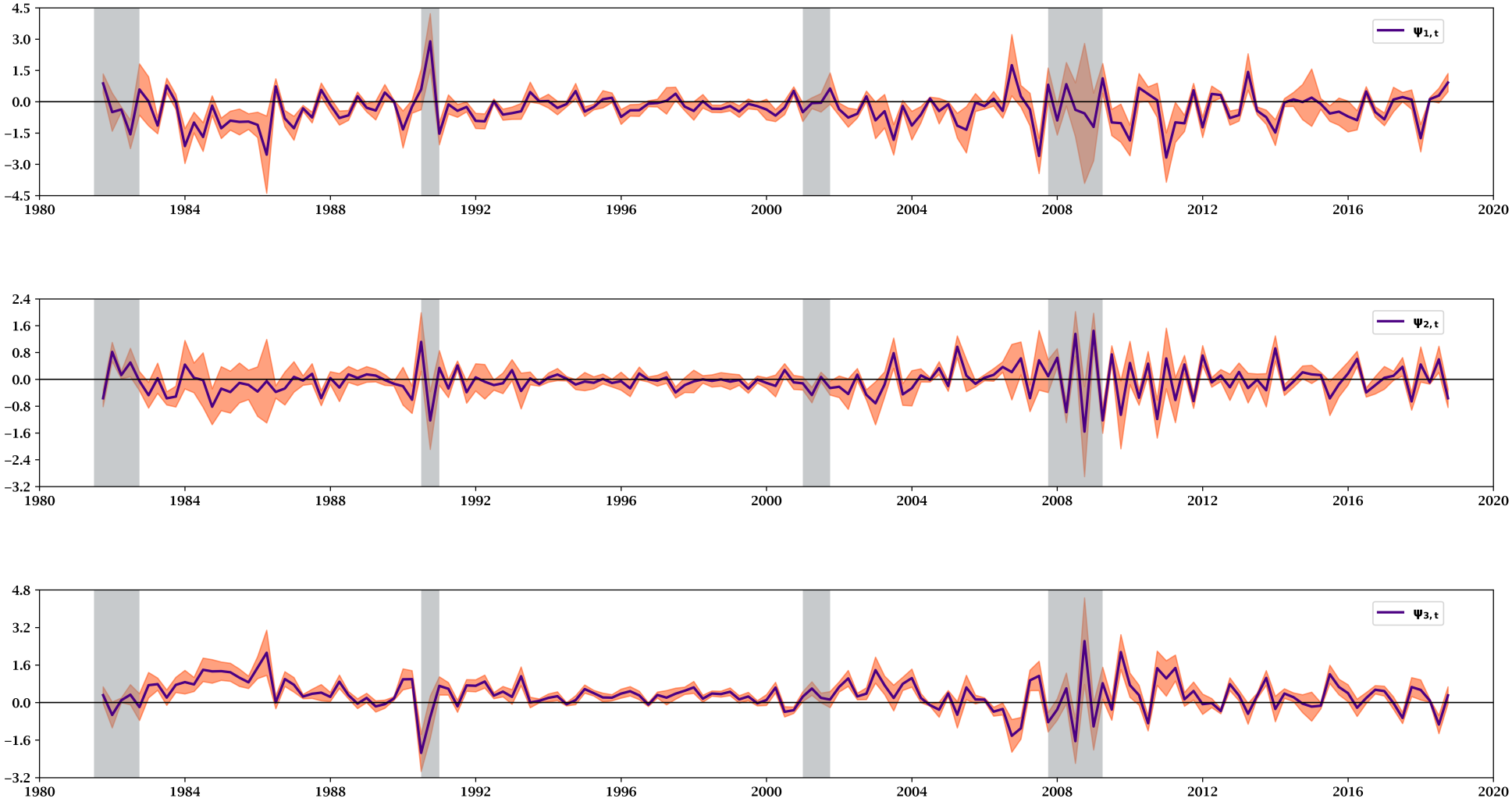

Note: Sixty-eight percent uncertainty bands cover the measurement errors $\psi_{1,t}$, $\psi_{2,t}$, and $\psi_{3,t}$. The plots also contain vertical gray bands that denote NBER dated recessions.

Figure A.2: $\mathcal{M}_{SI}$ Estimates of Measurement Errors, $\psi_{h,t}$, for $h = 1$, 2, and 3, on the PGNP/PGDP-SPF Sample, 1969Q1 to 2018Q4

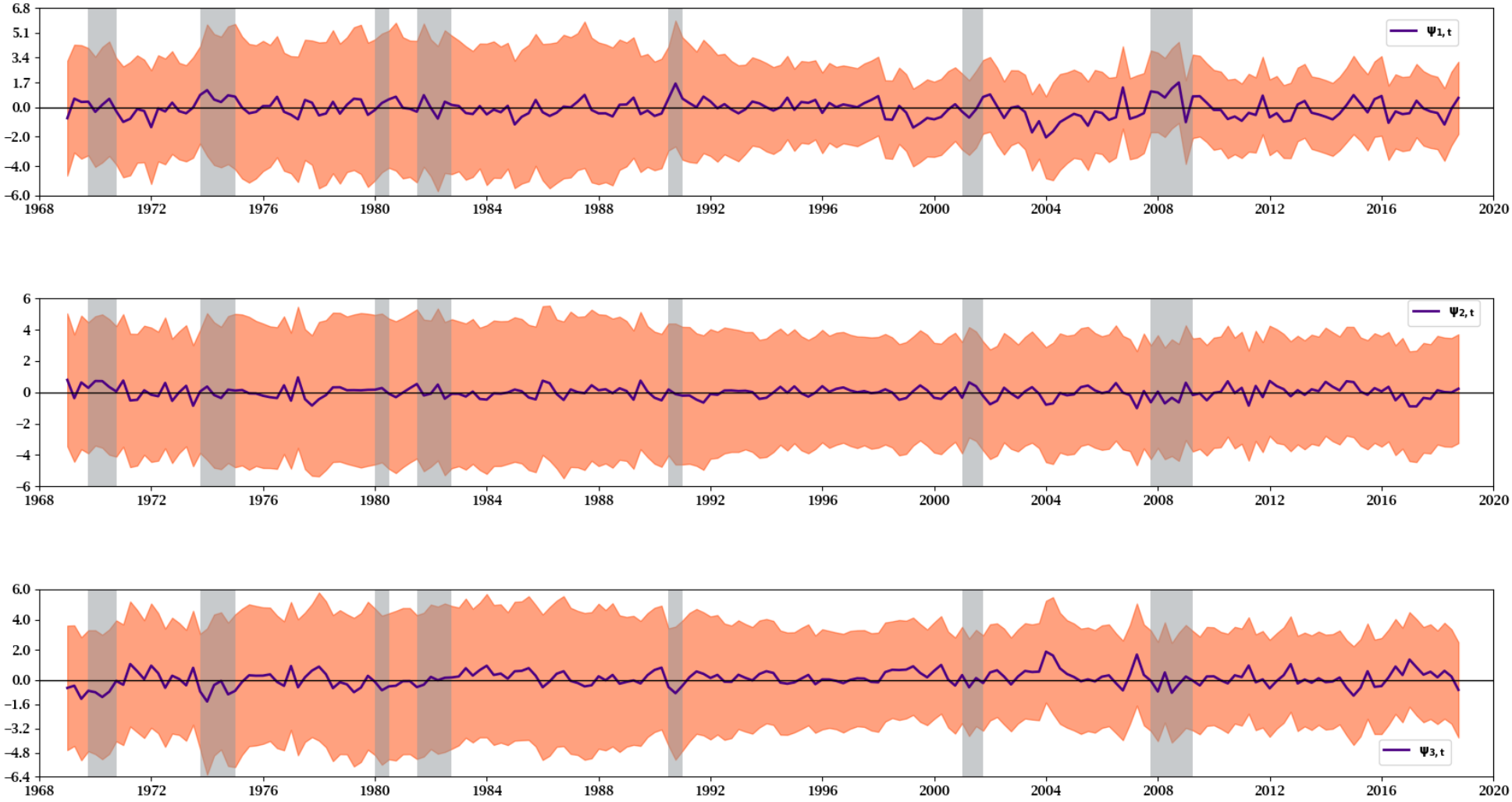

Note: Sixty-eight percent uncertainty bands cover the measurement errors $\psi_{1,t}$, $\psi_{2,t}$, and $\psi_{3,t}$. The plots also contain vertical gray bands that denote NBER dated recessions.